Journal of Alloys and Compounds 525 (2012) 82–86

Contents lists available at SciVerse ScienceDirect

Journal of Alloys and Compounds

journal homepage: www.elsevier.com/locate/jallcom

Enhanced microwave performance of highly ordered mesoporous carbon coated by Ni_2O_3 nanoparticles

Hongjing Wu*, Liuding Wang, Yiming Wang, Shaoli Guo, Zhongyuan Shen

Department of Applied Physics, School of Science, Northwestern Polytechnical University, Xi'an 710072, PR China

ARTICLE INFO

Article history:
Received 20 September 2011
Received in revised form
13 December 2011
Accepted 10 February 2012
Available online xxx

Keywords:
Ni/OMC
Microwave absorption
Impedance matching
Negative permeability

ABSTRACT

Electromagnetic and microwave absorbing properties of the ordered mesoporous carbon (OMC) doped by Ni_2O_3 nanoparticles absorber was investigated for the first time. A minimum reflection loss (RL) value of −39 dB at 10.9 GHz and a broad absorption band with the RL values under −10 dB is obtained in the whole Ku-band and X-band when the thickness is 2.0 mm and 2.8 mm, respectively. It showed far more excellent microwave absorbing properties with respect to undoped Ni_2O_3 OMC/paraffin composite. This phenomenon could be attributed to the strong cooperative effect between Ni_2O_3 and OMC.

1. Introduction

Since the first synthesis of ordered mesoporous carbon (OMC) named CMK-1 in 1999 by Ryoo et al. [1] the extensive investigations on OMC have shown that they possess a series of remarkable physico-chemical properties, e.g., good mechanic and thermal stability, unique electrical behavior, and special nanostructure composed of ordered nanowire arrays [2,3]. Especially a family of OMC named CMK-3 induced by SBA-15 template [4] has drawn more attention recently, which find application in many fields, such as adsorption and separation, catalysis, energy storage, and drug delivery [5]. More recently, OMC are considered good candidates for microwave applications due to their large dielectric loss, such as electromagnetic interference (EMI) shielding and electromagnetic (EM) wave absorbing [6–10]. Compared with magnetic absorbers, dielectric OMC absorbers are much more light-weight, but have much higher dielectric constants and in turn do not match up to their magnetic loss [11]. Furthermore, the electrical conductivity of OMC materials is generally high, so that the complex permeability of absorbers may decrease due to the eddy current effect induced by EM wave [12]. Concerning problems, it is necessary to reduce the permittivity and increase the resistivity of these dielectric materials.

Recent interest has been expanded to the metallic soft magnetic materials, which may be a potential candidate for microwave absorption in high frequency range due to their higher Snoek's limit compared with ferrites [13,14]. Consequently, many OMC materials with magnetic particles or compounds encapsulated in the pores or attached on the outer surface of OMC have been researched taking advantage of the dielectric properties of OMC and the cooperative effect with the soft magnetic particles of nanocomposites [8,12].

In this paper, we investigate the microwave absorbing performance of Ni-coated OMC nanocomposites on the basis of the following considerations. Firstly, OMC would like to be promising EM wave absorbing materials due to their dielectric properties. Secondly, the complex permittivity of OMC can be tuned by soft magnetic particles, which may lead to the formation of abundant vacancies [8,11]. Thirdly, the soft magnetic particles play important roles in improving the complex permeability owing to their large saturation magnetization and higher Snoek's limit [11–13]. Finally, the unique structure of OMC is favorable for dispersing Ni-based species, which could result in an induced magnetic moment due to the spin polarized charge transfer between OMC and magnetic particles [15].

2. Experimental

2.1. Materials

The triblock copolymer, EO20PO70EO20 (Pluronic 123) was purchased from BASF. Tetraethyl orthosilicate (TEOS), sucrose, $Ni(NO_3)_2$, H_2SO_4, HCl, ethanol, and NaOH were purchased from Sinopharm Chemical Reagent Co., Ltd. All chemicals were used as received without any further purification. Deionized water was used in all experiments.

* Corresponding author. Tel.: +86 29 8843 1664; fax: +86 29 8843 1664.
E-mail address: wuhongjing@mail.nwpu.edu.cn (H. Wu).

0925-8388/$ – see front matter © 2012 Elsevier B.V. All rights reserved.
doi:10.1016/j.jallcom.2012.02.078

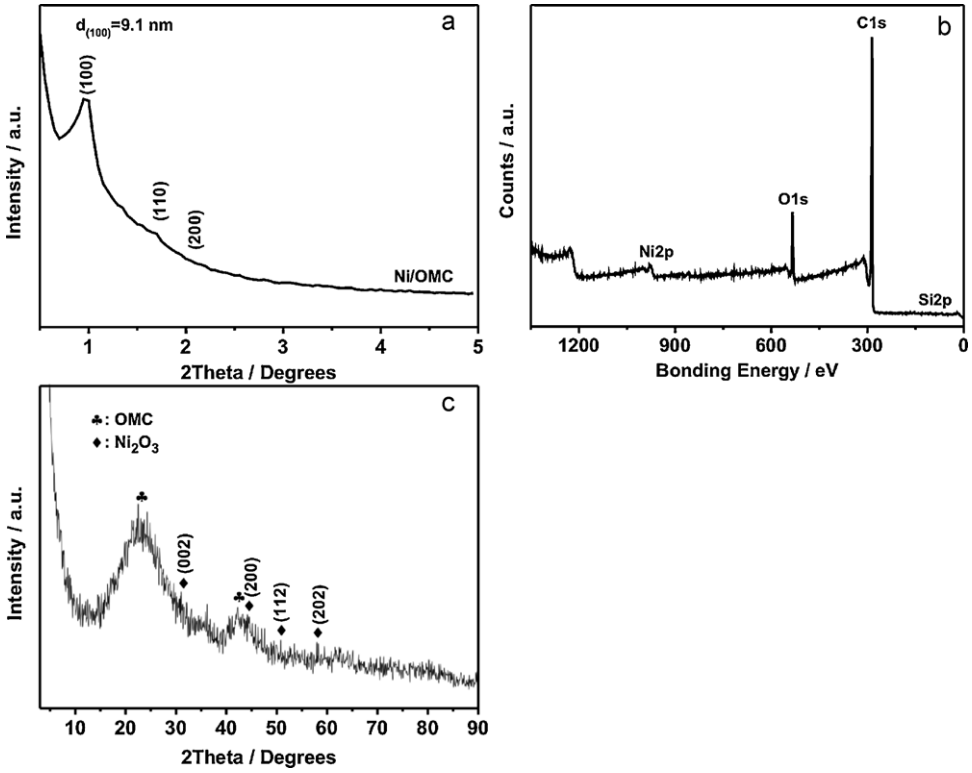

Fig. 1. (a) Low-angle XRD pattern and (b) full-range XPS spectrum of Ni/OMC composite.

2.2. Synthesis

Here mesoporous carbon was synthesized by using mesoporous silica (SBA-15) as hard template [3]. A high-quality SBA-15 sample was prepared by means of the triblock copolymer, EO20PO70EO20 (Pluronic 123, BASF), as the surfactant and tetraethyl orthosilicate (TEOS, 98%, Acros) as the silica source. Then, the calcined SBA-15 (1 g) was impregnated with a solution obtained by dissolving 1.25 g of sucrose and 0.14 g of H_2SO_4 in 5 g of water. The mixture was placed in a drying oven at 80 °C for 6 h, and subsequently the oven temperature was increased to 160 °C and maintained there for 6 h. After the treatment in the oven, the sample turned dark brown. The pretreated sample was treated again at 80 and 160 °C after the addition of 0.8 g of sucrose, 0.09 g of H_2SO_4 and 5 g of H_2O. The carbonization was completed by pyrolysis at 900 °C under N_2. The Ni/OMC nanocomposite was prepared by an ultrasonic irradiation method [16]. Typically, 0.5 g of OMC was added to 20 mL of a $Ni(NO_3)_2$ aqueous solution (0.10 mol/L), and then the mixture was ultrasonically irradiated at room temperature. After irradiation for 120 min, the Ni-containing OMC was filtered, washed thoroughly with deionized ethanol, and dried at 80 °C for 12 h. The so-obtained solid was thermally treated in a muffle furnace. The above procedure was repeated several times until the weight of the dried solid did not change. The resulting material was calcined at 300 °C for 4 h. The Ni/OMC/paraffin composite was prepared by ultrasonic agitation to mix a certain weight fraction (1:5) of Ni/OMC with paraffin.

2.3. Characterization

The prepared powder was pressed into a toroid with an outer diameter of 7.0 mm, inner diameter of 3.04 mm, and thickness of 3.0 mm. The complex permittivity and permeability data of Ni/OMC/paraffin composite was measured using a HP vector network analyzer (HP 8720B) in 2.0–18.0 GHz. The synthesized Ni/OMC composite was characterized by X-ray diffraction on a Rigaku D/MAX diffractometer (Cu Kα radiation, λ = 1.5406 Å). Scanning electron microscope was performed on a JEOL JSM-5610LV instrument. Transmission electron microscopy images were taken on a JEOL JEM-2100 instrument equipped with a Perkin-Elmer XPS spectrometer (ESCA PHI 5400). The binding energy (BE) for the samples was calibrated by setting the measured bonding energy of C1s to 284.60 eV. The magnetic properties of the product were performed on a Quantum Design MPMS-XL5 SQUID magnetometer. Magnetic hysteresis loop measurement was performed at T = 300 K.

3. Results and discussion

The low-angle XRD pattern of meso-Ni/OMC (Fig. 1a) shows a relatively sharp peak at $2\theta = 0.97°$ with two relatively weak peaks at around 2θ of 1.70 and 1.95°, which can be indexed to (1 0 0), (1 1 0), and (2 0 0) diffractions of the *p6mm* symmetry, respectively [3]. The intense (1 0 0) peak reflects a *d*-spacing of 9.1 nm corresponding to a unit-cell constant a_0 = 10.51 nm. The full-range spectrum, as shown in Fig. 1b, indicates that the elements on the surface of the sample are C (85.4 wt.%), O (12.4 wt.%), Ni (1.0 wt.%) and Si (1.2 wt.%), respectively. Three different C1s signals are observed at about 285 eV, 286 eV and 289 eV as shown in Fig. S1a. The main signal at 285 eV corresponds to C=C sp^2 bonds, indicating a surface graphitization after thermal process [17]. The signals at 286 eV and 289 eV are assigned to C=N and COOH, respectively, suggesting that carbon surface is covered by a large number of relatively weak electric groups, which may facilitate to increase the resistivity of Ni/OMC. XPS O1s spectrum displays a series of distinct peaks at 532.18 eV, 532.39 eV and 533.54 eV (Fig. S1b), which can be assigned to the electrophilic O-species (O_2^- or O^-) [18]. The $Ni2p_{3/2}$ peak is centered at 874.07 eV and the $Ni2p_{1/2}$ peak at 855.68 eV with a shakeup satellite at about 5.93 and 5.74 eV higher bonding energy values, respectively (Fig. S1c), which may be typical of Ni_2O_3 [19]. The results indicate that Ni-doped OMC is favorable for the formation of abundant weak electric groups and oxygen vacancies, contributing to reducing the complex permittivity and increasing the resistivity of the Ni/OMC composites. Fig. 1c shows the wide-angle XRD pattern of the Ni/OMC nanocomposites. It can be seen that some weak diffraction peaks corresponding to Ni_2O_3 (2θ = 31.9°, 44.8°, 51.6° and 56.8°, JCPDS data file 14-0481) are observed in the case of the as-synthesized Ni/OMC samples, suggesting that the Ni_2O_3 nanoparticles are in a very dispersion degree. In addition, the low weight fraction of Ni_2O_3 in the composites as indicated by the XPS analysis is also the reason for their weak diffraction peaks.

Fig. 2a and b shows TEM images of Ni/OMC viewed from different directions of the hexagonal pore arrangement, indicating the structure of the CMK-3 carbon is exactly an inverse replica of SBA-15. The TEM images in Fig. 2a and b show that the pore walls are 5.9 nm thick, the center of adjacent rods are 8.3 nm apart and then

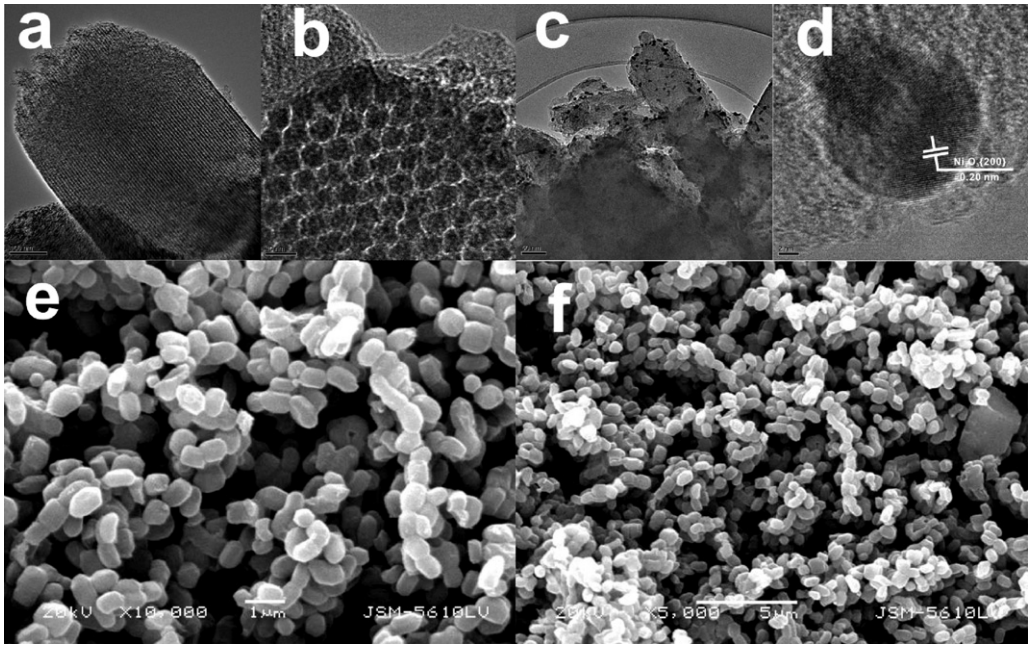

Fig. 2. The TEM (a–d) images and SEM (e and f) images of Ni/OMC composite.

the pore size is 2.4 nm. It can be seen that the Ni_2O_3 nanoparticles are well dispersed and the average particle size is 15.0 nm by the randomly statistical calculation in Fig. 2c. Fig. 2d shows the interplanar *d*-spacing (0.20 nm) corresponding to that of the {2 0 0} lattice planes of the Ni_2O_3. Furthermore, larger-scale carbon nanorods with average 490 nm in diameter and 1.18 μm in length are shown in Fig. 2e and f. It can be seen that the Ni_2O_3 nanoparticles coated on the OMC nanorod surface are hardly observed in SEM images with relatively low magnification.

Generally, the magnetic properties result from coupling between electron-spin and orbital angular momentum of the electrons at atomic level. The magnetization, as a function of the magnetic field strength of Ni/OMC nanocomposites at 300 K, is shown in Fig. 3. The saturation magnetization of the Ni/OMC is found to be much lower than that of the bulk Ni_2O_3, mainly due to the much low content of Ni element (1.0 wt.%) in the nanocomposites. The coercivity (H_c) of the nanocomposites is about 58 Oe (Fig. 3, inset), suggesting the existence of an effective anisotropy field of these nanoparticles in the nanocomposites. It is well-known that H_c approaches zero for very small particels because thermal fluctuations can prevent the existence of a stable magnetization.

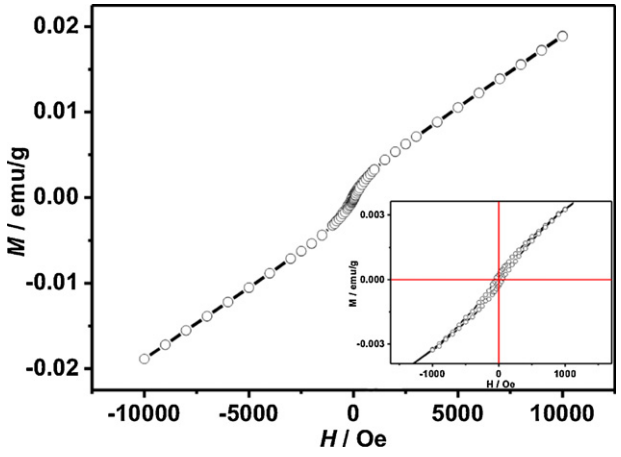

Fig. 3. The isothermal magnetization curve at 300 K.

It indicates that the thermal energy is not sufficient to overcome the anisotropy barrier of the orientation of a well-isolated single domain Ni_2O_3 particle at 300 K. The enhanced effective anisotropy energy value would influence the natural resonance frequency of the nanocomposites [12].

The frequency dependency on the real part (ε') and imaginary part (ε'') of the complex permittivity (ε_r for Ni/OMC/paraffin composites is shown in Fig. 4a. It can be found that the values of ε' declined from 11.2 to 4.3 over the 2.0–18.0 GHz frequency range. In addition, one peak can be observed near the resonance frequencies on the ε' curve. Meanwhile, a minimum value can be found at the corresponding resonance frequency on the ε'' curve. This phenomenon is ascribed to displacement current lag or before at the carbon nanorods or carbon nanorods/paraffin interfaces, which is similar to the case of Ni/ZnO nanocapsules [20].

The plot of ε' versus ε'', which is usually defined as the *cole–cole* semicircle, is shown in Fig. 4c. It is worthy to note that the Ni/OMC/paraffin composite presents a clear segment of one semicircle at high frequencies and a linear curve at relatively low frequencies, which is different from OMC/paraffin (Fig. S2a). The presence of semicircle suggests that there is a Debye dielectric relaxation process [20]. In addition to the dielectric relaxation process, other dielectric mechanisms such as resistance loss, interfacial polarization, and oxygen defects may contribute to the permittivity dispersion [21]. According to free-electron theory, $\varepsilon'' \approx 1/2\pi\varepsilon_0\rho f$, where ρ is the resistivity. It can be speculated that the lower ε'' value of the Ni/OMC indicates a higher resistivity with respect to the OMC (Fig. S2b), i.e., the average resistivity of the Ni/OMC is 47 Ω m, which is higher than that of OMC. This higher resistivity may be originated from the oxygen defects, weak electric conducting groups (C=N and COOH, respectively), and soft magnetic Ni_2O_3 on the surface of carbon nanorods, which may reduce the imaginary permittivity of the carbon materials. The resistance loss can also contribute to the dielectric loss of Ni/OMC/paraffin composite [11].

Fig. 4b shows the complex permeability of the Ni/OMC/paraffin composites. It can be seen that the real (μ') and imaginary (μ'') parts exhibit a natural resonance peak at near 4.0 GHz. According to the natural resonance equation $2\pi f_r = \gamma H_a$, where $\gamma = 2.8$ GHz/kOe is the gyromagnetic ratio and $H_a = 4|K_1|$, the anisotropic coefficient

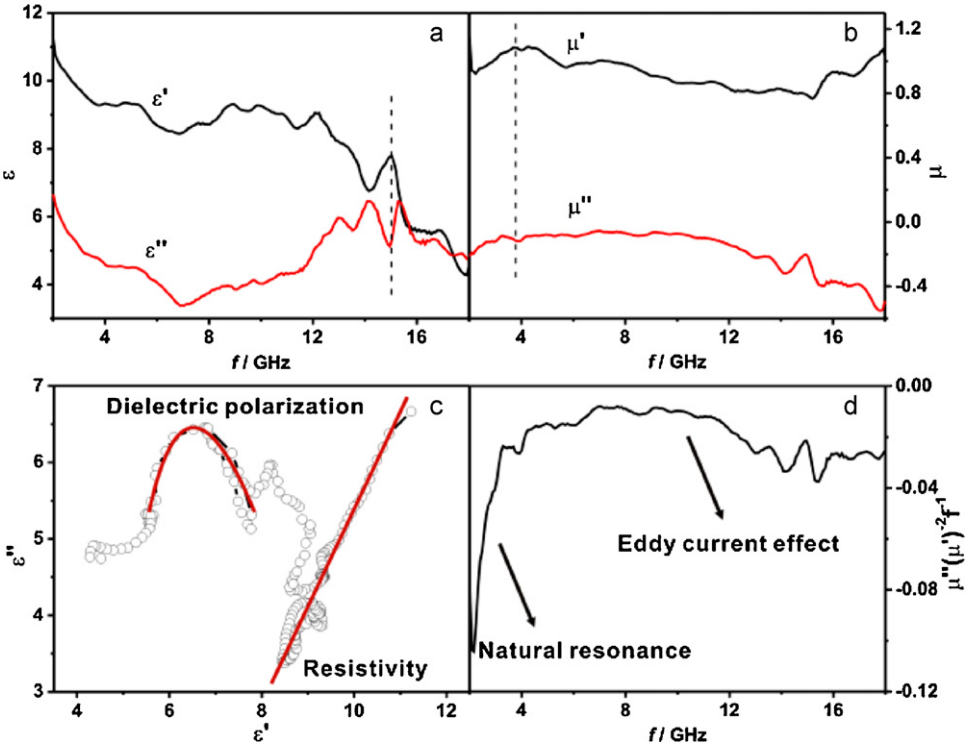

Fig. 4. (a) Complex permittivity and (b) permeability, (c) Cole–Cole semicircles and (d) values of $\mu''(\mu')^{-2}f^{-1}$ as a function of frequency for Ni/OMC.

(K_1) for the fcc-type bulk nickel which is about -5×10^3 J/m^3, [22] the natural resonance frequency should be around several tens of megahertz [11]. However, in the present paper, the fact that resonance frequency shifts to the higher frequency (4.0 GHz) may be due to the nanosize effect, which leads to the increase of the anisotropic energy of ultra-fine Ni_2O_3 by reducing the magnetic coupling among them as discussed in Fig. 3.

It can be inferred that magnetic hysteresis, domain-wall displacement are excluded in the present Ni/OMC sample because of weak applied field and single domain structure of the nanosized Ni-based species in our work [12]. Although the soft magnetic Ni_2O_3 has higher Snoek's limit, a little eddy current loss may be present in our sample. Fig. 4d shows the value of $\mu''(\mu')^{-2}f^{-1}$ as a function of frequency. The value of $\mu''(\mu')^{-2}f^{-1}$ first increases sharply and then keeps nearly constant as the frequency is increased. If the magnetic loss only results from eddy current loss the value of $\mu''(\mu')^{-2}f^{-1}$ should be a constant when the frequency is varied. Therefore, we can infer that the eddy current loss could contribute to magnetic loss at relatively high frequencies. Besides, the eddy currents can produce an induced magnetic field, which opposes the applied field and in turn radiates EM wave, leading to the increase of the total magnetic energy and a negative imaginary permeability at high frequencies (Fig. 4b) [8,10]. The induced magnetic energy may contribute the complementary magnetic loss with a conversion of incident wave to other forms of energy.

Fig. 5 shows the dissipation factors represented by the dielectric loss ($\tan\delta_e$) and magnetic loss ($\tan\delta_m$) of the Ni/OMC/paraffin composites. The $\tan\delta_e$ increases significantly with three peaks at about 14.0, 16.0 and 18.0 GHz, respectively. Meanwhile, the change trend of $\tan\delta_m$ is just inverse to that of $\tan\delta_e$, which can be explained by the LRC equivalent circuit model, where L, R and C are the inductance, resistance and capacitance, respectively. In the case of Ni/OMC, the Debye dielectric dipolar relaxation plays a role as capacitance; the interface polarization and resistance loss, etc. act as resistance; and the fact that the eddy current loss produces an induced magnetic field in the microwave absorbing process can be regarded as the inductance. From Fig. 5, the inverse change trend between C and L is attributed to the capacitance leading or lagging behind the angle of 90° than the inductance [23]. Conversely, the dielectric loss of OMC/paraffin may be mainly determined by leak conductance, which corresponds to CG model (Fig. S2c), where G is conductance.

To further prove the proper match affected by the microstructure of absorber, the reflection loss (RL) of Ni/OMC/paraffin was calculated according to transmission line theory [24] (see Supporting Materials), as shown in Fig. 6. It is shown that the minimum RL reaches −39.0 dB at 10.9 GHz and the absorption range under −10 dB is obtained in the whole Ku-band and X-band with 2.0 mm and 2.8 mm thickness layers, respectively. Additionally, the microwave absorption properties of C-Al_2O_3, [7] C-SiO_2-Fe, [8] C-TiO_2, [9] C-Fe_2O_3, [10] and C-Ni_2O_3 are summarized in Table 1. The RL values for C-Ni_2O_3 are comparable to that of above-mentioned metal-doped OMC nanocomposites. Moreover,

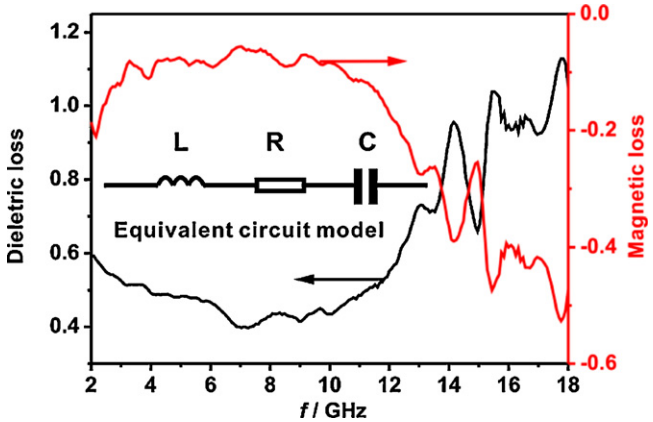

Fig. 5. Frequency dependencies of dielectric and magnetic factors of Ni/OMC (the inset shows the equivalent circuit model).

Table 1
EM wave absorbing properties of some metal-doped OMC nanocomposites.

Sample	Optimal RL value (dB)	d_m (mm) (RL < −10 dB)	f_m (GHz) (optimal RL)	Frequency range (GHz) (RL < −10 dB)	References
C-Al_2O_3	−15.3	3	11.5	7.4	[7]
C-SiO_2–Fe	−34.4	2	13.1	5.0	[8]
C-TiO_2	−25.4	3	13	6.6	[9]
C-Fe_2O_3	−32	3	6.4	2.0	[10]
C-Ni_2O_3	−34	2	15	5.5	This work

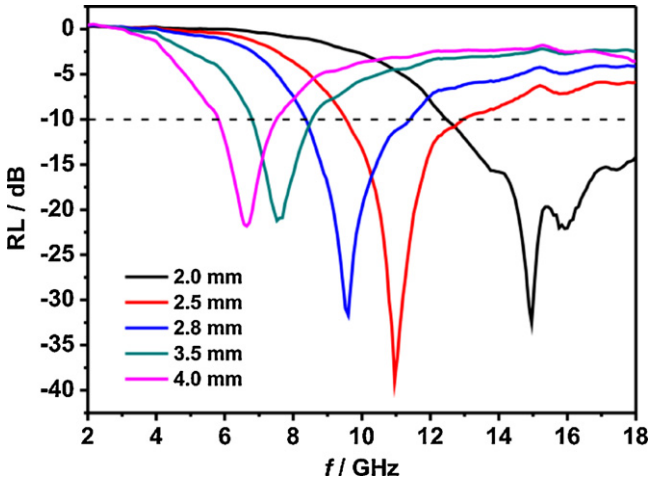

Fig. 6. Frequency dependence of the RL values of the Ni/OMC with different thicknesses.

The Ni-coated OMC nanocomposites possess relatively broader frequency range (RL ≤ −10 dB) with the thin absorber matching thickness, i.e., d_m = 2 mm, which can be regarded as effective absorbing materials in practical applications. By comparing the EM properties of pure OMC (Fig. S2d), enhanced EM properties are ascribed to the cooperative effect between Ni_2O_3 nanoparticles and meso-carbon nanorods.

4. Conclusions

In summary, the Ni/OMC/paraffin composite exhibits excellent EM absorption properties, which are attributed to the dielectric resonance, resistance loss, natural resonance and eddy current loss. The light-weight Ni/OMC may become a promising candidate for EM absorbing material.

Acknowledgements

This project was supported financially by the National Natural Science Foundation of China (nos. 50771082 and 60776822) and the graduate starting seed fund of Northwestern Polytechnical University (no. Z2011011).

Appendix A. Supplementary data

Supplementary data associated with this article can be found, in the online version, at doi:10.1016/j.jallcom.2012.02.078.

References

[1] R. Ryoo, S.H. Joo, J.M. Kim, J. Phys. Chem. B 103 (1999) 7435–7440.
[2] J. Lee, J. Kim, T. Hyeon, Adv. Mater. 18 (2006) 2073–2094.
[3] S. Jun, S.H. Joo, R. Ryoo, M. Kruk, M. Jaroniec, Z. Liu, T. Ohsuna, O. Terasaki, J. Am. Chem. Soc. 122 (2000) 10712–10713.
[4] D.Y. Zhao, J.L. Feng, Q.S. Huo, N. Melosh, G.H. Fredrichson, B.F. Chmelka, G.D. Stucky, Science 279 (1998) 548–552.
[5] A.H. Lu, F. Schüth, Adv. Mater. 18 (2006) 1793–1805.
[6] J.C. Wang, C.S. Xiang, Q. Liu, Y.B. Pan, J.K. Guo, Adv. Funct. Mater. 18 (2008) 2995–3002.
[7] T. Wang, J.P. He, J.H. Zhou, X.C. Ding, J.Q. Zhao, S.C. Wu, Y.X. Guo, Micropor. Mesopor. Mater. 134 (2010) 58–64.
[8] J.H. Zhou, J.P. He, G.X. Li, T. Wang, D. Sun, X.C. Ding, J.Q. Zhao, S.C. Wu, J. Phys. Chem. C 114 (2010) 7611–7617.
[9] T. Wang, J.P. He, J.H. Zhou, J. Tang, Y.X. Guo, X.C. Ding, S.C. Wu, J.Q. Zhao, J. Solid State Chem. 183 (2010) 2797–2804.
[10] J.H. Zhou, J.P. He, T. Wang, G.X. Li, Y.X. Guo, J.Q. Zhao, Y. Ma, J. Alloys Compd. 509 (2011) 8211–8214.
[11] Q.L. Liu, D. Zhang, T.X. Fan, Appl. Phys. Lett. 93 (2008) 013110–13113.
[12] X.F. Zhang, X.L. Dong, H. Huang, Y.Y. Liu, W.N. Wang, X.G. Zhu, B. Lv, J.P. Lei, C.G. Lee, Appl. Phys. Lett. 89 (2006) 053115–53123.
[13] J.L. Snoek, Physica 14 (1948) 207–217.
[14] V.B. Bregar, IEEE Trans. Magn. 40 (2004) 1679–1684.
[15] O. Cespedes, M. Ferreira, S. Sanvito, M. Kociak, J. Coey, J. Phys.: Condens. Mater. 16 (2004) L115–L123.
[16] J.G. Deng, L. Zhang, H.X. Dai, Y.S. Xia, H.Y. Jiang, H. Zhang, H. He, J. Phys. Chem. C 114 (2010) 2694–2700.
[17] C. Weidenthaler, A.H. Lu, W. Schmidt, F. Schüth, Micropor. Mesopor. Mater. 88 (2006) 238–243.
[18] M.M. Natile, A. Glisenti, Chem. Mater. 14 (2002) 3090–3099.
[19] B.W. Hoffer, A.D.V. Langeveld, J.P. Janssens, R.L.C. Bonné, C.M. Lok, J.A. Moulijn, J. Catal. 192 (2000) 432–440.
[20] X.G. Liu, J.J. Jiang, D.Y. Geng, B.Q. Li, Z. Han, W. Liu, Z.D. Zhang, Appl. Phys. Lett. 94 (2009) 053119–53123.
[21] P.C.P. Watts, W.K. Hsu, A. Barnes, B. Chambers, Adv. Mater. 15 (2003) 600–603.
[22] L.L.P. Diandra, D.R. Reuben, Chem. Mater. 8 (1996) 1770–1783.
[23] X.L. Shi, M.S. Cao, J. Yuan, X.Y. Fang, Appl. Phys. Lett. 95 (2009) 163108–163113.
[24] E. Michielssen, J. Sajer, S. Ranjithan, R. Mittra, I.E.E.E Trans, Microwave Theory Technol. 41 (1993) 1024–1031.